Double Ionization to CO_2 Produces Molecular Oxygen: A Roaming Mechanism

Qibo Ma(马启博)†, Xintai Hao(郝鑫泰)†, Jiaqi Zhou(周家琪)*, Xiaorui Xue(薛晓睿), Qingrui Zeng(曾庆睿), Peng Li(李鹏), Lei Wang(王磊), and Xueguang Ren(任雪光)*

Ministry of Education Key Laboratory for Nonequilibrium Synthesis and Modulation of Condensed Matter, School of Physics, Xi'an Jiaotong University, Xi'an 710049, China

(Received 24 September 2025; accepted manuscript online 24 November 2025)

Abiotic oxygen formation predates photosynthesis, sustaining early chemical evolution, yet its elementary mechanisms remain contested. Here, we show the production pathways for molecular oxygen from doubly ionized carbon dioxide upon electron-impact. Through fragment ions and electron coincidence momentum imaging, we unambiguously determine the ionization mechanism by measuring the projectile energy loss in association with the $C^+ + O_2^+$ channel. Further potential energy and trajectory calculations enable us to elucidate the dynamical details of this fragmentation process, in which a bond rearrangement pathway is found to proceed via the structural deformation to a triangular intermediate. Moreover, we demonstrate a further roaming pathway for the formation of O_2^+ from CO_2^{2+}, in which a frustrated C-O bond cleavage leaves the O atom without sufficient energy to escape. The O atom then wanders around varied configuration spaces of the flat potential energy regions and forms a C-O-O^{2+} intermediate prior to the final products $C^+ + O_2^+$. Considering the large quantities of free electrons in interstellar space, the processes revealed here are expected to be significant and should be incorporated into atmospheric evolution models.

DOI: 10.1088/0256-307X/43/1/010301 CSTR: 32039.14.0256-307X.43.1.010301

Molecular oxygen (O_2), as a crucial component of the Earth's atmosphere, is the cornerstone of life-sustaining processes. Prior to the Great Oxygenation Event caused by photosynthetic oxygen production,[1–4] abiotic processes dominated Earth's primordial oxygen budget, providing O_2 required for the earliest chemical evolution of life. Over the past decades, the combination of two O atoms via three-body collisions ($O + O + M \rightarrow O_2 + M$) has been widely recognized as the main abiotic pathway for O_2 production,[5–7] in which a third body (M) is involved to carry away the excess energy. The O atoms are generated through the dissociation of CO_2 or other precursor molecules.[8–11]

In recent years, studies on abiotic O_2 sources have identified direct O_2-production routes from CO_2 via intrinsic structural transformation, without requiring atomic O intermediates. Theoretical calculations first predicted the possibility of producing O_2 from CO_2,[12,13] which was then demonstrated by the experimental work of Lu *et al.*[14] This study revealed the O_2 formation pathway via vacuum ultraviolet photodissociation of CO_2 ($h\nu + CO_2 \rightarrow C + O_2$). Later, dissociative electron attachment ($e^- + CO_2 \rightarrow C^- + O_2$) and He^+ ion-induced charge exchange ($He^+ + CO_2 \rightarrow O_2 + C^+ + He$) processes have been identified as further pathways to produce neutral O_2 from CO_2.[15,16] Moreover, the dissociation processes of doubly- and singly-charged CO_2 ions forming cationic O_2^+ ($CO_2^{2+}/CO_2^+ \rightarrow C^+/C + O_2^+$) have also been identified, which can be efficiently converted into abiotic O_2 through electron neutralization or charge exchange.[16–24] These results significantly advance our understanding of the Earth's atmospheric evolution, and provide more insights into planetary atmospheres and interstellar chemical processes. During the O_2/O_2^+ generation, a fascinating question arises concerning how a linear O-C-O molecule could eliminate its central C atom to produce O-O bonding molecules.

For excited CO_2 molecules, there are two mechanisms for central C elimination: one involves dissociation from a transition state (TS) accessed by prior bending deformation of the molecule and the other invokes breakage of one C-O bond followed by intramolecular roaming.[12–14] Since its first observation in 2004, roaming reactions have been established as a generic aspect of chemical reactivity.[25] Evidence of roaming dynamics has been observed across diverse molecular systems involving various fragments.[26–33] In the O roaming pathway, after one C-O bond breaks, the O atom without enough energy to escape and orbits the remaining fragment until encountering a reactive site to form a C-O-O isomer through intramolecular abstraction. In the case of ionized CO_2, only the former mechanism has been proposed,[18,23] whereas the roaming pathway remains unexplored for the dicationic CO_2^{2+}, both experimentally and theoretically. Recent electron-impact absolute cross section measurements indicate that double ionization of CO_2 molecule can contribute considerably to the

†These authors contributed equally to this work.

*Corresponding authors. Email: zhoujiaqi@xjtu.edu.cn; renxueguang@xjtu.edu.cn

© 2026 Chinese Physical Society and IOP Publishing Ltd. All rights, including for text and data mining, AI training, and similar technologies, are reserved.

O_2^+ production.[20] However, the mechanistic and dynamical details of this O_2^+ formation process still need to be elucidated.

In this work, we present new insights into the production of O_2^+ from doubly ionized CO_2 by electron-impact with an energy of 200 eV, representative of a subset of free electrons detected in Mar's atmosphere.[34,35] We also notice here that doubly-charged ions are readily formed by direct ionization and Auger processes in the planetary atmospheres as they are always exposed to ionizing radiations.[34–38] We study the two-body ($C^+ + O_2^+$) fragmentation channel of CO_2 using a multi-particle coincidence momentum spectrometer via a cold target recoil ion momentum spectroscopy or reaction microscope[39,40] combined with a pulsed photoemission electron source, in which the momentum vectors of two fragment ions are measured in coincidence with the scattered electron.[40,41] The ionization mechanism is determined by measuring the projectile energy loss spectrum in association with the $C^+ + O_2^+$ channel, which shows two obvious structures in the kinetic energy release (KER) spectrum. Furthermore, we performed potential energy surface (PES) calculations and classic trajectory simulations of the $C^+ + O_2^+$ channel, which enable us to elucidate the dynamical details of the reaction pathways, particularly for a new roaming mechanism.

In the experiment, the time-of-flight (TOF) and position of fragment ions and electrons were recorded with two position- and time-sensitive multihit detectors, which allows the offline determination of mass-to-charge ratios, momentum vectors, and kinetic energies for all three charged particles [see Supplementary Materials (SM)]. We first characterize O_2^+ production from CO_2^{2+} dication by the ion-ion TOF correlation map. As shown in Fig. 1, two correlated fragments originating from the same precursor molecule show a clear TOF correlation due to momentum conservation, which manifests as a sharp line with a slope of -1.[42,43] The most intense channel in Fig. 1 is assigned to $O^+ + CO^+$, while the adjacent channel on the left corresponds to $C^+ + O_2^+$, which provides definitive evidence of O_2^+ production from CO_2^{2+}. In addition, isotope channels $^{17}O^+ + CO^+$ and $^{18}O^+ + CO^+$ are also clearly resolved. The yield of the $C^+ + O_2^+$ channel is approximately 0.174% that of the $O^+ + CO^+$ channel, consistent with previous strong-field laser and ion collision experiments.[18,23]

To identify the initial state of CO_2^{2+} dications that produce O_2^+, we measured the projectile energy loss ($E_{\rm loss}$) spectrum of the $C^+ + O_2^+$ channel. Here, $E_{\rm loss}$ is defined as the energy difference between incident electron (E_0) and scattered electron (E_1), which determines the minimum ionization energy for a specific channel. Figure 2 displays the measured $E_{\rm loss}$ spectrum of the $C^+ + O_2^+$ channel, which is calibrated with the known double-ionization energy of CO_2 ($E_{\rm loss}[CO_2^{2+}] = 37.3$ eV).[44,45] The onset of the $E_{\rm loss}$ spectrum (as indicated by the red arrow at ~42.0 eV) corresponds to the $^3\Pi_u$ dicationic excited state,

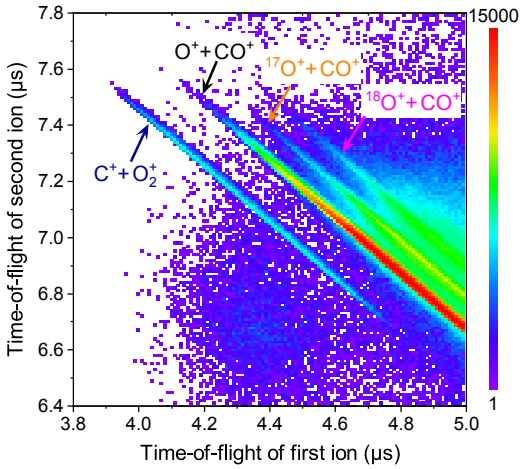

Fig. 1. Measured two ions TOF correlation map of the two-body dissociation of CO_2^{2+}, in which the $O^+ + CO^+$ and $C^+ + O_2^+$ channels are clearly identified. The isotope channels $^{17}O^+ + CO^+$ and $^{18}O^+ + CO^+$ are also clearly resolved.

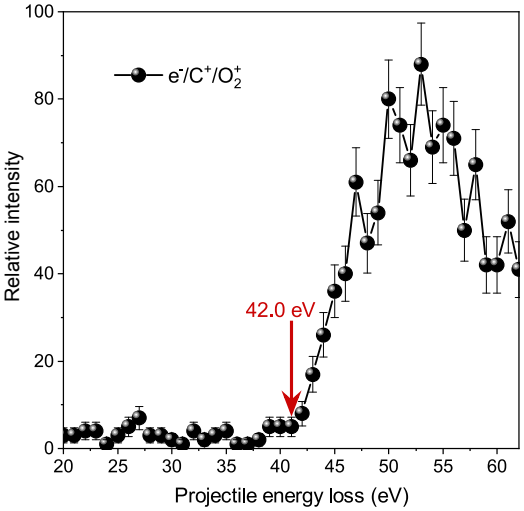

Fig. 2. Projectile energy loss spectrum of the $C^+ + O_2^+$ channel obtained by electron-ion-ion triple-coincidence measurement. The red arrow indicates the onset of the spectrum.

which is attributed to the ejections of one electron from the highest occupied molecular orbital (HOMO) and the other from HOMO-2.[44,45] In electron-impact experiments, this state can be accessed either through direct double ionization or via inner-shell ionization of the $3\sigma_{1g}/2\sigma_{2u}$ orbitals followed by Auger processes.[46] Recent cross-section analysis of O_2^+ formed by electron-impact with CO_2 indicates that parent CO_2^{2+} ions originate predominantly from Auger processes.[22]

To form O_2^+ from CO_2^{2+} dication, a bond rearrangement pathway has been proposed in which the symmetrical stretching and bending of the two C-O bonds lead to the reduced ∠O-C-O and subsequently new bond formation between the two O atoms.[18,23] However, the dynamics governing the formation of O_2^+ via CO_2^{2+} remain elusive, particularly for the question of whether the roaming mechanism can play a role in this reaction. This pathway necessitates the cleavage of one C-O bond and the formation of a C-O-O^{2+} intermediate with an intramolecular

O abstraction prior to the $C^+ + O_2^+$ dissociation process. In order to elucidate the dynamics of O_2^+ formation from CO_2^{2+}, we have performed *ab initio* calculations on the reaction coordinate of $CO_2^{2+} \rightarrow C^+ + O_2^+$. Our calculations were carried out using the Minnesota 2006 hybrid meta-exchange-correlation functional with double the amount of non-local exchange (2X) (M062X) method and the aug-cc-pVTZ basis set.[47,48] The relative energies of all TSs and intermediate states (INs) are corrected with zero point energy using the CCSD/aug-cc-pVTZ method.[49] The intrinsic reaction coordinate calculations were also performed to verify reaction pathways linking TS to local minima (see SM).

The calculated potential energies for the reaction from the CO_2^{2+} dicationic states to the final products $C^+ + O_2^+$ are presented in Fig. 3. For the reaction corresponding to the singlet state ($a^1\Delta_g^+$) of CO_2^{2+} [shown in Fig. 3(a)], we first determine the vertical ionization energy to be 39.19 eV, which is in good agreement with previous studies.[44,45] After double ionization to the singlet state, the CO_2^{2+} dicationic molecule can relax to the local lowest energy state (LES), then rearrange significantly the molecular structure with stretching and bending deformations through a transition state TS1, during which the distance between the two O atoms decreases to 1.68 Å. In the intermediate state IN1, the CO_2^{2+} dication adopts a triangular structure, with the ∠O-C-O angle and the O-O bond distance being 41.8° and 1.18 Å, respectively. This structural rearrangement leads to the formation of a new O-O covalent bond. The bending deformation has been proven to be very fast and can be completed in just a few femtoseconds.[19] The intermediate state IN1 is characterized by weakened C-O bonds, which consequently leads to fragmentation with an extremely low energy barrier of only 0.05 eV (TS2), resulting in the final products $C^+ + O_2^+$. This small energy barrier suggests that the fragmentation process is highly favorable and proceeds efficiently once the IN1 state is reached.

In addition to the bond rearrangement pathway revealed in Fig. 3(a), we identify a further roaming mechanism for the formation of O_2^+ from CO_2^{2+}. As shown in Fig. 3(b), the roaming pathway is initiated by the population on the triplet state ($X^3\Sigma_g^-$) of CO_2^{2+}. The calculated vertical ionization energy of the $X^3\Sigma_g^-$ state amounts to 37.3 eV, which is consistent with the double ionization threshold of CO_2 determined by experimental

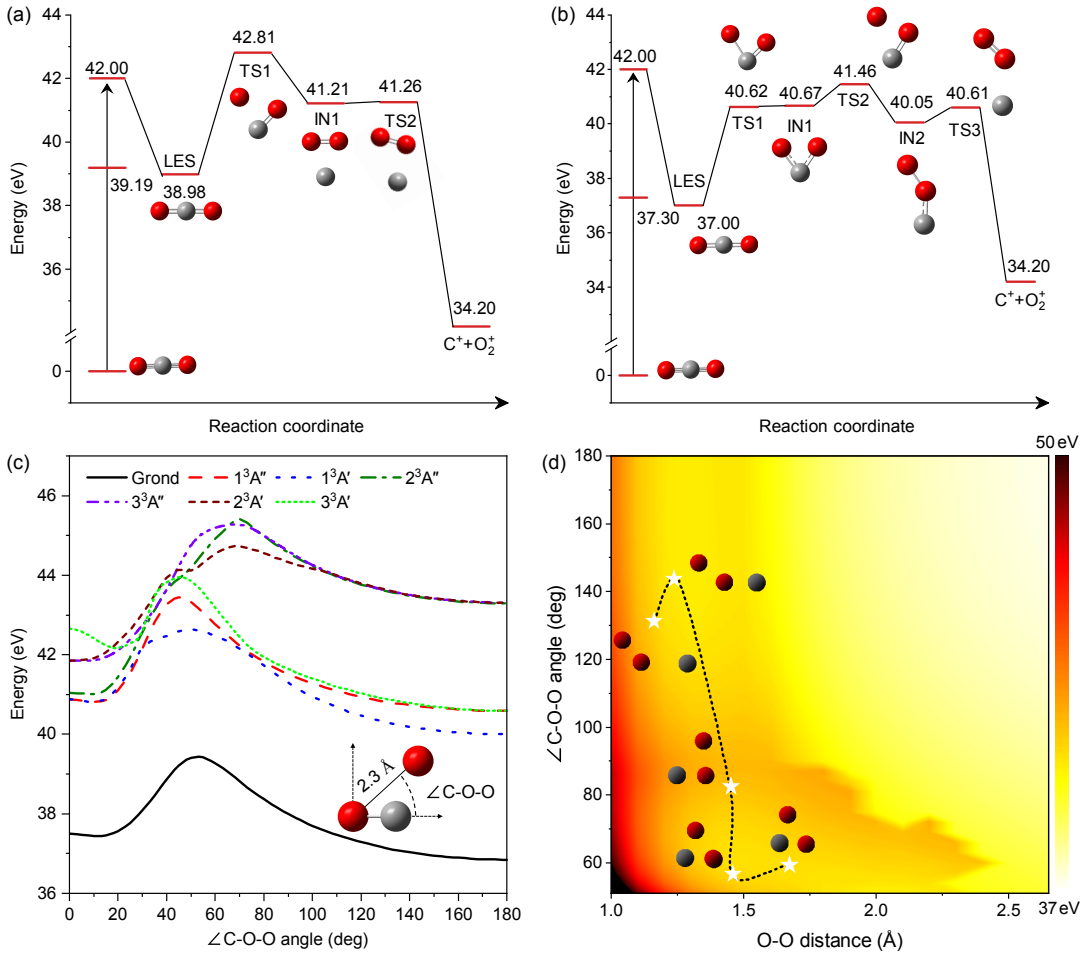

Fig. 3. Calculated reaction pathways with the selected TSs and INs along the potential energy curves of the $C^+ + O_2^+$ channel from the singlet (a) and triplet (b) states of CO_2^{2+}. (c) Potential energy curves of different triplet states of CO_2^{2+} by varying ∠C-O-O angle from 0° to 180°. (d) Two-dimensional PES as a function of the ∠C-O-O angle and O-O distance. The dotted line indicates the roaming path, in which the white five-pointed stars represent the TSs and INs shown in (b).

and theoretical studies.[44,45] Upon double ionization and relaxation to the local LES, the CO_2^{2+} dication then crosses the first transition state (TS1) and reaches a metastable intermediate state IN1, which is characterized by a remarkable structural rearrangement. At this stage, the initially linear O-C-O backbone experiences a drastic angular deformation, bending from 180° to 67.5°, along with a substantial contraction of the O···O internuclear distance from its equilibrium value of 2.32 Å to 1.44 Å. The CO_2^{2+} subsequently progresses toward the second transition state (TS2). Here, the charge redistribution results in a significant weakening of the C-O bond, ultimately leading to its complete cleavage. This quasifree O atom, which does not have enough energy to escape, rotates around the C-O moiety and ultimately recombines with it at a suitable reaction site (IN2), forming a C-O-O^{2+} isomer. This newly formed O-O bond adopts an equilibrium distance of 1.25 Å, and the accompanying ∠C-O-O angle opens to 143.5°. The C-O-O^{2+} dication further crosses an energy barrier of approximately 0.6 eV (TS3), leading to the breakage of the C-O bond and the formation of $C^+ + O_2{}^+$ ion pairs. It is noted in Fig. 3(b) that the potential energies of TSs and INs from TS1 to TS3 are very close, thereby posing a flat PES, which is essential for O roaming and ultimately the abstracting of another O to form an oxygen molecule. Here, all TSs lie energetically below the initial $^3\Pi_u$ state, enabling a barrierless roaming process. A similar O roaming mechanism has been identified in SO_2^{2+} as an alternative O_2^+ production route to the bending vibrational pathway,[30] and it is proposed that similar situations should also apply to CO_2^{2+}.[20] However, there are fundamental differences between SO_2 and CO_2, e.g., in molecular structure, electronic state and so on. The O roaming mechanism in CO_2^{2+} need to be verified experimentally. The electronically excited CO_2^{2+} ($^3\Pi_u$) undergoes internal conversion to the triplet state PES, the O atom then wanders around varied configuration spaces of the flat potential energy regions and forms a C-O-O^{2+} intermediate prior to the final products $C^+ + O_2^+$.

This roaming mechanism is further illustrated in Fig. 3(c), where we calculate the potential energy landscape in a coordinate system that displaces one O atom relative to the other while varying the ∠C-O-O angle. The O-O bond distance is fixed at 2.3 Å, matching the equilibrium distance in neutral CO_2 (see SM). For the ground and the excited $1^3A'$ states of the CO_2^{2+} dication, the potential barriers lie below the initial $^3\Pi_u$ state, enabling CO_2^{2+} convert from a bent O-C-O^{2+} configuration to a linear C-O-O^{2+} isomer by crossing a potential barrier. Furthermore, the $1^3A''$ state may undergo a roaming-mediated O_2^+ formation through conical intersection with the $1^3A'$ potential energy curve. The higher excited states exhibit O-roaming barriers above the initial $^3\Pi_u$ state, rendering roaming dynamics unlikely. The roaming pathway is visualized clearly by our calculated two-dimensional PES as a function of the ∠C-O-O angle and O-O distance shown in Fig. 3(d). Since the roaming originates from TS1 in Fig. 3(b), we map the PES starting from 50° of the ∠C-O-O angle. The corresponding TSs and INs from Fig. 3(b) are also marked in Fig. 3(d) to trace the roaming pathway, which exhibits a flat potential energy profile. Along the indicated pathway, potential barriers exist on both sides as the O-O distance increases or decreases. The potential energy of the CO_2^{2+} dication decreases as the ∠C-O-O angle increases. This leads to the breaking of a C-O bond and subsequent roaming of the O atom around the C-O moiety while keeping the O-O distance constant when increasing the ∠C-O-O angle. When the ∠C-O-O angle reaches approximately 143°, the roaming O atom recombines with the C-O moiety, forming a C-O-O structure. Finally, the C-O bond breaks, yielding the final products $C^+ + O_2^+$. Upon crossing the potential barriers along the O-O coordinate, the C-O-O^{2+} intermediate will rapidly dissociate into $O^+ + CO^+$.

According to the energy differences between the final TS and the ion products in Fig. 3, it should lead to different KER distributions for O_2^+ production from the bond rearrangement and roaming pathways. As shown in Fig. 4, the different KER distributions are resolved in our measured KER spectrum of the $C^+ + O_2^+$ channel, which exhibits two dominant peaks centered at about 6.4 eV and 7.6 eV, respectively. We utilize Gaussian fitting to resolve the two KER distributions, obtaining a branching ratio of 55% : 45% between the two peaks. The low-energy KER peak agrees well with the result measured by strong-field laser ionization[18] and ion collision[23] experiments. This double-peak structure was previously observed in O 1s→ π^* excited $C^+ + O_2^+$,[19] which confirms that the O_2^+ production from CO_2^{2+} primarily arises from the Auger process in this work. The singlet CO_2^{2+} state is produced predominantly through Auger autoionization, while the triplet CO_2^{2+} state originates mainly from direct double ionization.[50] As the incident electron energy increases, this Auger-to-direct-ionization cross-section ratio increases.[20] Consequently, the proportion of the KER component associated with O-roaming and bond rearrangement pathways is expected to systematically increase with increasing electron energy. The energy difference between TS3 and the ionic products in Fig. 3(b) is determined to be 6.41 eV, which is in good agreement with the low-energy KER peak. This indicates that the low-energy KER peak primarily arises from the roaming pathway. While the peak located at KER ∼7.6 eV is close to the energy difference between TS2 and the ionic products (7.06 eV) in Fig. 3(a), which indicates that the high-energy KER peak is mainly attributed to the bond rearrangement pathway of CO_2^{2+}.

To further quantify the KER distributions, we carried out molecular dynamics calculations using a classical trajectory method (see SM), in which the known molecular structures are used as input parameters to calculate the KER distributions of the ion pair.[51–53] During the structural evolution of the singlet and triplet states in CO_2^{2+}, we obtained two different pre-dissociation TS configurations.

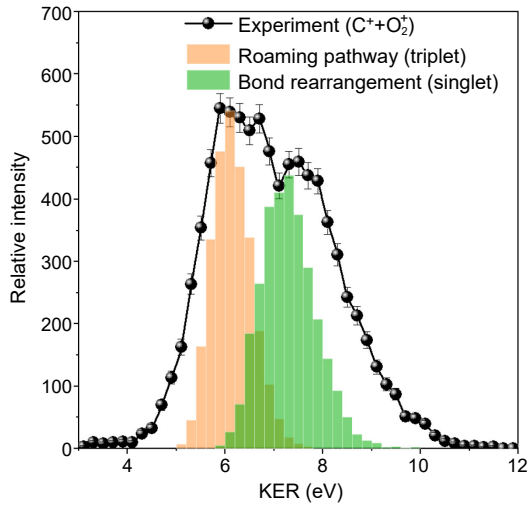

Fig. 4. Measured KER spectrum for the $C^+ + O_2^+$ channel. The orange and green bar distributions represent the KER spectra calculated with the Coulomb explosion model applied to charge separation using the triplet-state (TS3) and singlet-state (TS2) transition structures, respectively.

For the triplet state, a nearly linear transition state (TS3) was identified, characterized by an associated O-O bond length of 1.15 Å and a connected C-O bond length of 1.84 Å. The singlet state adopts a bent transition state (TS2), featuring an ∠O-C-O bond angle of 93° and an O-O bond length of 1.16 Å. By setting the vibrational full width at half maximum (FWHM) of the C-O and O-O bond lengths to 0.3 Å and the angular FWHM of the ∠C-O-O (and ∠O-C-O) to 30°, we calculate the KER distributions for two reaction pathways, which are displayed by the orange (triplet state) and green (singlet state) bar charts in Fig. 4. The calculated KER distributions response well to the double-peak structure in the experimental spectrum. This result supports again that the two peaks in the KER spectrum originate from the bond rearrangement and roaming pathways, respectively.

In conclusion, we have studied experimentally and theoretically the production of O_2^+ from doubly ionized CO_2 molecule upon electron-impact, where O_2^+ can be converted to O_2 by electron recombination or charge exchange processes.[30] Using fragment ions and electron coincidence momentum spectroscopy, we have obtained the projectile energy loss spectrum in association with the $C^+ + O_2^+$ dissociation channel, which provide unambiguous evidence for the mechanism of the $^3\Pi_u$ excited state-controlled fragmentation of CO_2^{2+} dication. Further potential energy and trajectory calculations have elucidated the fragmentation dynamics of the production of O_2^+ from CO_2^{2+}, which shows good agreement with the measured KER spectrum of $C^+ + O_2^+$ products. Our studies have revealed the dynamical details of the bond rearrangement pathway, in which an intermediate triangular structure is formed after population of the singlet state of CO_2^{2+}. This pathway likely contributes to the high energy (7.6 eV) peak of the KER spectrum.

Moreover, we demonstrate a further roaming mechanism for the formation of O_2^+ from CO_2^{2+}, which is found to be a barrierless pathway. This roaming pathway is initiated by double ionization and relaxation to the triplet state, then a frustrated C-O bond cleavage leaves the O atom without sufficient energy to escape. Subsequently, the O atom wanders around varied configuration spaces of the flat potential energy regions and forms a C-O-O^{2+} intermediate prior to the final products $C^+ + O_2^+$ (KER ∼6.4 eV). The abundance of free electrons in interstellar space and the upper atmosphere suggests that the processes revealed here are significant and should be incorporated into atmospheric chemistry models. The present studies provide new insights into the abiotic oxygen generation in CO_2-rich planetary atmospheres and facilitate the identification of hitherto unrecognized pathways of interstellar chemistry and molecular evolution within the universe.

Acknowledgements. This work was jointly supported by the National Natural Science Foundation of China (Grant Nos. 12325406, 92261201, 12404305, and W2512072), the Shaanxi Province Natural Science Fundamental Research Project (Grant Nos. 2023JC-XJ-03 and 23JSQ013), and the China Postdoctoral Science Foundation (Grant Nos. BX20240286 and 2024M7625).

References

[1] Lyons T W, Reinhard C T and Planavsky N J 2014 *Nature* **506** 307
[2] Bekker A, Holland H D, Wang P L, Rumle D, Stein H J, Hannah J L, Coetzee L L, and Beukes N J 2004 *Nature* **427** 117
[3] Kasting J F 1993 *Science* **259** 920
[4] Canfield D 2005 *Annu. Rev. Earth Planet. Sci.* **33** 1
[5] Harman C E, Schwieterman E W, Schottelkotte J C, and Kasting J F 2015 *Astrophys. J.* **812** 37
[6] Kasting J F, Pollack J B, and Crisp D 1984 *J. Atmos. Chem.* **1** 403
[7] Kasting J F and Walker J C G 1981 *J. Geophys. Res. Oceans* **86** 1147
[8] Feng Q, Tian S X, Zhao Y J, Liu F Y, Shan X B, and Sheng L S 2009 *Chin. Phys. Lett.* **26** 053402
[9] Zhang S, Xia Y Q, Wang Y Q, Lu Z Z, and Chen D Y 2009 *Chin. Phys. Lett.* **26** 083202
[10] Hu S L, Zhao Z X, and Shi T Y 2013 *Chin. Phys. Lett.* **30** 103103
[11] Zhang J F, Ma R, Zuo W L, Lv H, Huang H W, Xu H F, Jin M X, and Ding D J 2015 *Chin. Phys. B* **24** 033302
[12] Hwang D Y and Mebel A M 2000 *Chem. Phys.* **256** 169
[13] Grebenshchikov S Y 2013 *J. Chem. Phys.* **138** 224106
[14] Lu Z, Chang Y, Yin Q Z, Ng C, and Jackson W 2014 *Science* **346** 61
[15] Wang X D, Gao X F, Xuan C J, and Tian S X 2016 *Nat. Chem.* **8** 258
[16] Zhi Y Y, Guo Q, Xie J C, Hu J, and Tian S X 2023 *Commun. Chem.* **6** 267
[17] Zhao S, Jochim B, Feizollah P, Rajput J, Ziaee F, Raju P K, Kaderiya B, Borne K, Malakar Y, Berry B, Harrington J, Rolles D, Rudenko A, Carnes K D, Wells E, Ben-Itzhak I, and Severt T 2019 *Phys. Rev. A* **99** 053412
[18] Larimian S, Erattupuzha S, Mai S, Marquetand P, González L, Baltuska A, Kitzler M, and Xie X H 2017 *Phys. Rev. A* **95** 011404

[19] Laksman J, Månsson E P, Grunewald C, Sankari A, Gisselbrecht M, Céolin D, and Sorensen S L 2012 *J. Chem. Phys.* **136** 104303

[20] Monteiro-Carvalho A B, Sigaud L, and Montenegro E C 2024 *Phys. Rev. Lett.* **132** 153002

[21] Eland J H D, Zagorodskikh S, Squibb R J, Mucke M, Sorensen S L, and Feifel R 2014 *J. Chem. Phys.* **140** 184305

[22] Ganguly S, Barreiro-Lage D, Walsh N, Oostenrijk B, Sorensen S L, Díaz-Tendero S, and Gisselbrecht M 2022 *Commun. Chem.* **5** 16

[23] Kumar K, Mukherjee J, Singh H, and Misra D 2024 *Atoms* **12** 25

[24] Dong R C, Chen A H, Feng J Z, Zhang S, Jiang W B, Hu X Q, Wu Y, Wang J G, Wang X C, and Jiang Y H 2024 *Phys. Rev. A* **110** 053110

[25] Townsend D, Lahankar S A, Lee S K, Chambreau S D, Suits A G, Zhang X, Rheinecker J, Harding L B, and Bowman J M 2004 *Science* **306** 1158

[26] Quinn M S, Nauta K, Jordan M J T, Bowman J M, Houston P L, and Kable S H 2020 *Science* **369** 1592

[27] Foley C D, Xie C J, Guo H, and Suits A G 2021 *Science* **374** 1122

[28] Endo T, Neville S P, Wanie V, Beaulieu S, Qu C, Deschamps J, Lassonde P, Schmidt B E, Fujise H, Fushitani M, Hishikawa A, Houston P L, Bowman J M, Schuurman M S, Lgar F, and Ibrahim H 2020 *Science* **370** 1072

[29] Wang E L, Ren X G, and Dorn A 2021 *Phys. Rev. Lett.* **126** 103402

[30] Wallner M, Jarraya M, Olsson E, Idebhn V, Squibb R J, Yaghlane S B, Nyman G, Eland J H, Feifel R, and Hochlaf M 2022 *Sci. Adv.* **8** eabq5411

[31] Li Z X, Fu Y L, Luo Z J, Yang S J, Wu Y C, Wu H, Wu G R, Zhang W Q, Fu B N, Yuan K J, Zhang D H, and Yang X M 2024 *Science* **383** 746

[32] Chang Y, Ashfold M, Yuan K J, and Yang X M 2023 *Natl. Sci. Rev.* **10** nwad158

[33] Jin W W, Wang C C, Zhao X G, Yang Y Z, Ren D X, Liu Z J, Li X K, Luo S Z, and Ding D J 2024 *Chin. Phys. Lett.* **41** 053101

[34] Mitchell L D, Mazelle C, Sauvaud J A, Thocaven J J, Rouzaud J, Fedorov A, Rouger P, Toublanc D, Taylor E, Gordon D, Robinson M, Heavner S, Turin P, Diaz-Aguado M, Curtis D W, Lin R P, and Jakosky B M 2016 *Space Sci. Rev.* **200** 495

[35] Peterson W K, Thiemann E M B, Eparvier F G, Andersson L, Fowler C M, Larson D, Mitchell D, Mazelle C, Fontenla J, Evans J S, Xu S, Liemohn M, Bougher S, Sakai S, Cravens T E, Elrod M K, Benna M, Mahaffy P, and Jakosky B 2016 *J. Geophys. Res. Space Physics* **121** 8859

[36] Thissen R, Witasse O, Dutuit O, Wedlund C S, Gronoff G, and Lilensten J 2011 *Phys. Chem. Chem. Phys.* **13** 18264

[37] Feldman W C, Asbridge J R, Bame S J, Montgomery M D, and Gary S P 1975 *J. Geophys. Res. Space Physics* **80** 4181

[38] Stverářák S, Trávnícek P, and Hellinger P 2015 *J. Geophys. Res. Space Physics* **120** 8177

[39] Dörner R, Mergel V, Jagutzki O, Spielberger L, Ullrich J, Moshammer R, and Schmidt-Böcking H 2000 *Phys. Rep.* **330** 95

[40] Ullrich J, Moshammer R, Dorn A, Dörner R, Schmidt L P H, and Schmidt-Böcking H 2003 *Rep. Prog. Phys.* **66** 1463

[41] Ren X G, Zhou J Q, Wang E L, Yang T, Xu Z F, Nicolas S, Thomas P, and Dorn A 2022 *Nat. Chem.* **14** 232

[42] Zhou J Q, Wu L, Belina M, Skitnevskaya A D, Jia S K, Xue X R, Hao X T, Zeng Q R, Ma Q B, Zhao Y T, Li X K, He L H, Luo S Z, Zhang D D, Wang C C, Trofimov A B, Slavicek P, Ding D J, and Ren X G 2025 *Nat. Commun.* **16** 5848

[43] Yu X T, Hu X Q, Zhou J Q, Zhang X Y, Zhao X N, Jia S K, Xue X R, Ren D X, Li X K, Wu Y, Ren X G, Luo S Z, and Ding D J 2022 *Chin. Phys. Lett.* **39** 113301

[44] Eland J H D 2003 *Chem. Phys.* **294** 171

[45] Zhang D W, Chen B Z, Huang M B, Meng Q Y, and Tian Z Y 2013 *J. Chem. Phys.* **139** 174305

[46] Hwang W, Kim Y, and Rudd M E 1996 *J. Chem. Phys.* **104** 2956

[47] Becke A D 1993 *J. Chem. Phys.* **98** 5648

[48] Lee C, Yang W T, and Parr R G 1988 *Phys. Rev. B* **37** 785

[49] Goings J J, Caricato M, Frisch J F, and Li X S 2014 *J. Chem. Phys.* **141** 164116

[50] Eland J H D, Plogmaker S, Lablanquie P, Penent F, Palaudoux J, Nicolas C, Robert E, Miron C, and Feifel R 2016 *Chem. Phys. Lett.* **646** 31

[51] Hsieh S and Eland J H D 1995 *J. Chem. Phys.* **103** 1006

[52] Hsieh S and Eland J H D 1997 *J. Phys. B: At. Mol. Opt. Phys.* **30** 4515

[53] Eland J H D and Sheahan J R 1994 *Chem. Phys. Lett.* **223** 531